JGR Planets

RESEARCH ARTICLE
10.1029/2018JE005772

Geomorphological Evidence of Localized Stagnant Ice Deposits in Terra Cimmeria, Mars

Solmaz Adeli[1], Ernst Hauber[1], Gregory G. Michael[2], Peter Fawdon[3], Isaac B. Smith[4,5], and Ralf Jaumann[1,2]

[1]Institut für Planetenforschung, Deutsches Zentrum für Luft- und Raumfahrt (DLR), Berlin, Germany, [2]Institut für Geowissenschaften, Freie Universität Berlin, Berlin, Germany, [3]School of Physical Sciences, Open University, Milton Keynes, UK, [4]Planetary Science Institute, Lakewood, CO, USA, [5]Lassonde School of Engineering, York University, Toronto, Ontario, Canada

Key Points:
- Small debris-covered stagnant ice deposits (termed valley fill deposits or VFD) are located inside a valley system in Terra Cimmeria, Mars
- Morphological properties (convex upward morphology, crevasses, and sublimation pits) suggest a current degradational stage of VFD evolution
- The location of VFD within the ejecta blanket of Middle Amazonian Tarq crater points to impact into shallow ice as a likely formation process

Supporting Information:
- Supporting Information S1
- Data Set S1

Correspondence to:
S. Adeli,
solmaz.adeli@dlr.de

Citation:
Adeli, S., Hauber, E., Michael, G. G., Fawdon, P., Smith, I. B., & Jaumann, R. (2019). Geomorphological evidence of localized stagnant ice deposits in Terra Cimmeria, Mars. *Journal of Geophysical Research: Planets*, *124*, 1525–1541. https://doi.org/10.1029/2018JE005772

Received 1 AUG 2018
Accepted 11 APR 2019
Accepted article online 16 APR 2019
Published online 12 JUN 2019

Abstract The presence of snow and ice at midlatitudes of Mars cannot be explained by current climatic conditions, as surface ice is unstable. However, a large variety of debris-covered glaciers have been observed at both midlatitudes. Here, we report the presence of local, small-scale, and debris-covered stagnant ice deposits on the floor of a valley system in Terra Cimmeria. These deposits, termed valley fill deposits (VFD), have a distribution that is restricted to the host valley floor and to the extent of the ejecta blanket associated with Tarq impact crater. The VFD are characterized by convex-upward morphology, various crevasses, sublimation pits, an average area of a few square kilometers, and occasional ejecta streaks on their surface. Our model age estimation points to two possible time frames for the Tarq impact event; thus, we suggest two formation scenarios for VFD: (I) distribution of ice due to impact into shallow ice during the Middle Amazonian and (II) post-impact deposition of VFD due to precipitation. In both scenarios, ice preservation is most likely due to a lag of dust and debris deposited in the valley's topographic lows. Scenario I is more consistent with our geomorphological observation of the VFD being overlain by ejecta streaks. Our results highlight the importance of local geological events and conditions in the distribution and preservation of buried ice deposits on Mars and suggest that more small-scale and debris-covered ice deposits may exist in the midlatitudes than previously thought. These deposits are of high importance for future human exploration missions to Mars.

Plain Language Summary In the last two decades with the increase of high-resolution imagery data, more studies report the presence of ice deposits covered by dust and debris on the Martian surface, in both midlatitudes. These deposits must have been formed under different atmospheric conditions, since water ice is not stable in the current surface environment. One of the generally accepted hypotheses for their formation is precipitation induced by variations of Mars' axial tilt known as obliquity. During high obliquity phases, ice would have sublimated from the poles and redeposited in the midlatitudes. Here, we report the presence of small-scale ice deposits, located on the floor of a valley system in Terra Cimmeria. Although it is clear that these deposits were formed in different climatic conditions, their formation seems to be related to an impact into a shallow subsurface ice layer, redistributing a mixture of ejected material and ice across the region around the impact site. This study shows the importance of local geological processes, for example, impact cratering, in investigations of water ice distribution on Mars. Near-surface ice reservoirs are of high importance in the search for life and for future human exploration on Mars.

1. Introduction

Geomorphological and geophysical evidence suggest the presence of debris-covered glaciers in the midlatitude regions of Mars (±30° to ±60°; e.g., Dickson et al., 2008; Fassett et al., 2014; Hauber et al., 2008; Head et al., 2003; Hubbard et al., 2014; Levy et al., 2014; Souness et al., 2012). These glacial landforms include lobate debris aprons (LDA; Mangold, 2003), lineated valley fill (LVF; Head et al., 2006), concentric crater fill (CCF; Levy et al., 2010), and viscous flow features (Milliken et al., 2003). Their formation time frame varies among different studies, but they are generally believed to have formed during the Middle to Late Amazonian (e.g.Berman et al., 2015, Head et al., 2005, 2010, Mangold, 2003, Parsons & Holt, 2016). The main geomorphological evidence pointing to their glacial origin is their convex upward topographic profile and deformation patterns resulting from downslope flow of the material (Head et al., 2010). Additionally, data

from subsurface investigations by the SHAllow RADar sounding experiment indicate that these features are composed of ice buried below a layer of debris (Holt et al., 2008; Levy et al., 2014; Plaut et al., 2009). These former glaciers are thought to be remnants of more extensive ice layers and glaciers accumulated in both midlatitude regions by snow and ice deposition due to obliquity variations (Forget et al., 2006; Laskar et al., 2004; Madeleine et al., 2009).

Ice in midlatitude regions of Mars has been detected at both shallow (~1–2 m) and greater depth (a few tens of meters). The Phoenix lander detected two distinct types of ice at middle to high latitudes (68°N): ice-cemented regolith and ground ice (>90% of purity; Mellon et al., 2009; Cull et al., 2010). Fresh impact craters uncover the presence of shallow buried ice in the midlatitudes (Byrne et al., 2009; Dundas et al., 2014), and subsurface radar reflections reveal the presence of debris-covered glaciers (Holt et al., 2008; Plaut et al., 2009). However, it is still unclear whether the small-scale debris-covered glaciers on the surface have a similar origin, age, and formation mechanism to the deeper excess ice (Dundas et al., 2018). The formation and distribution of debris-covered glaciers are controlled by the climate and therefore provide a unique record of the past and recent climate of Mars (e.g., Forget et al., 2006).

Over the past 20 Myr, Mars' obliquity variations caused significant changes in the Martian seasonal cycles (Laskar et al., 2004). Head et al. (2003) hypothesize an ice age between 2.1 and 0.4 Ma ago, when the obliquity exceeded 30° and water ice was removed from the polar regions and transported to midlatitudes, where a thin mantle of ice-dust covered the surface. The end of this ice age is recorded by the rapid accumulation of north polar layered deposits resulting from the retreat of ice from the midlatitudes (Smith et al., 2016). Although obliquity variations cannot be calculated for periods more than 20 Ma ago (Laskar et al., 2004), it is likely that the surface of Mars repeatedly experienced such climate changes leading to cycles of deposition and sublimation/evaporation of ice and glacial deposits (e.g.Head et al., 2005, Smith et al., 2016). Global circulation models suggest that periods of high obliquity (>30°) may have caused the mobilization of polar volatiles and water vapor in the atmosphere toward the equator and therefore redeposition of ice and snow in lower latitudes (Forget et al., 2006; Madeleine et al., 2009; Mischna et al., 2003). They show that, during low obliquity phases, ice and snow are transported back to the poles (Greve et al., 2010; Levrard et al., 2007; Madeleine et al., 2012; Smith et al., 2016).

Here we describe geomorphological observations of well-preserved and previously unreported debris-covered ice deposits (hereafter referred to as valley fill deposits or VFD) in Terra Cimmeria (Figure 1). These VFD are located approximately 100 km south of the Sirenum Fossae, and within the extent of the ejecta blanket of the 35 km-diameter Tarq impact crater (this impact crater is named after the city Tarq (Persian: طرق) in Iran) at about 38°S and 173°E (Figure 1a). They are located on the floor of a valley system that was previously associated with Early to Middle Amazonian-aged fluvial activity (Adeli et al., 2016). The VFD are evidence of the local distribution of ice during the Amazonian and emphasize the role of local and regional processes in the distribution and preservation of surface ice covered by a lag of debris and dust. Investigating these small-scale deposits enables a better understanding of ice deposition and degradation and, thus, the mechanisms of preservation and may contribute to our understanding of the Middle and Late Amazonian climate, although at local scale. Constraining the distribution and volume of accessible surface and shallow buried ice reservoirs will also identify potential local habitable niches and special regions (Rettberg et al., 2016), as well as inform the selection of landing sites for future in situ resource utilization and human exploration missions to Mars.

2. Data and Method

In this study, we used a multi–data set approach with a combination of various image and topographic data enabling us to investigate surface features at a range of scales. Images from the High Resolution Stereo Camera (HRSC) (10–40 m per pixel; Jaumann et al., 2007; Gwinner et al., 2016) on board the Mars Express orbiter were used for understanding the geological context and regional setting of the study area. In addition to the images, digital elevation models (DEM; typical ground sampling distances of 50 to 100 m) derived from HRSC stereo images were used.

Context Camera (CTX) images (Malin et al., 2007) from the Mars Reconnaissance Orbiter (MRO), with a ground pixel size of ~6 m, were used for more local analyses. Several images acquired through the High Resolution Imaging Science Experiment (HiRISE, 25 cm/pixel; McEwen et al., 2007) were also used to

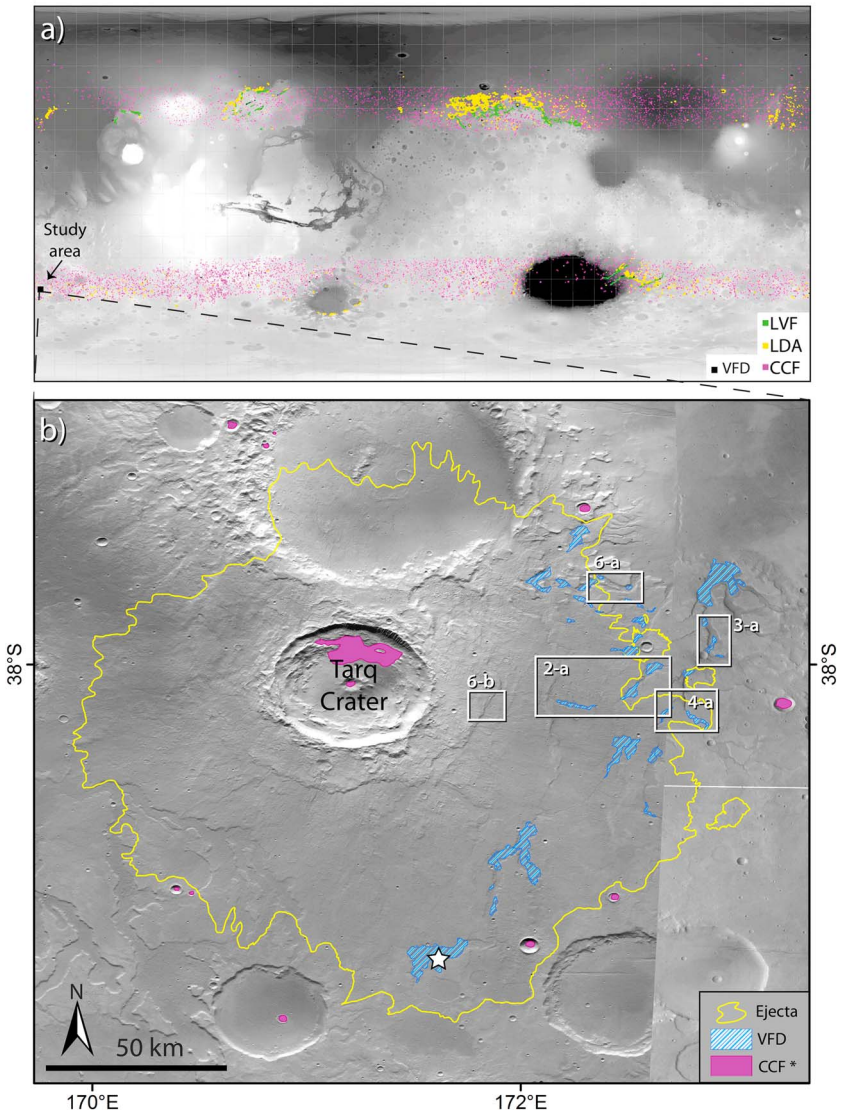

Figure 1. Study area. (a) Global distribution of LVF, LDA, and CCF shown on a MOLA map (modified after Levy et al., 2014) in addition to the VFD location reported in this study. (b) Valley system in Terra Cimmeria with VFD indicated in hachured blue lines. *The pink filled polygons represent the location of glaciers (only CCF located in our study area) mapped by Levy et al. (2014). The boundary of mapped ejecta blanket from Tarq crater is shown in yellow line (detail of HRSC nadir image, orbit numbers 12939 and 4198). The white star shows the approximate location of the VFD related to SHAllow RADar detection in Figure S1. The location of some figures in this study are marked. CCF = concentric crater fill; LDA = lobate debris apron; LVF = lineated valley fill; VFD = valley fill deposit.

study the detailed surface texture of the VFD, as well as one HiRISE DEM. The HiRISE DEM was created using the Integrated Software for Imaging Spectrometers (ISIS) and SocetSet following the methodology of Kirk et al. (2008) with a postspacing of ~1 m. The vertical precision of the HiRISE DEM was controlled by Mars Orbital Laser Altimeter (MOLA; Zuber et al., 1992) data.

One hyperspectral image cube of the Compact Reconnaissance Imaging Spectrometer for Mars (CRISM; Murchie et al., 2007) on board MRO (cube number: FRT16872) covers one of the deposits of interest in this paper. We analyzed this CRISM data with the aim of investigating the composition of the superficial material and potentially the underlying deposits (in case of an observation window). However, our spectral analysis of the infrared and visible spectra indicates the presence of dust in the area and did not show the occurrence of any spectral feature relevant to this study.

We analyzed 33 observations from the SHAllow RADar (SHARAD; Seu et al., 2007) instrument on MRO that cross the region of interest. In one of these observations we detected a possible subsurface reflector, which may correspond to the results discussed in this paper. The radar profile (supporting information Figure S1) was interpreted in several steps as explained in supporting information S1.

We also determined the absolute model ages of the regions of interest. We analyzed crater size-frequency distributions (CSFD) on CTX and HiRISE images at a scale of 1:24,000 in a GIS environment. Craters were mapped using the Crater-Tools (Kneissl et al., 2011) extension for the ArcGIS software. The Craterstats 2 software (Michael & Neukum, 2010) was used to model crater-based ages based on the chronology function of Hartmann and Neukum (2001) and the production function of Ivanov (2001). The results are plotted in a differential presentation of the CSFD. The data files used to produce the CSFD plots and fits are available as supporting information Data Set S1. Crater chronology model ages are derived here using the Poisson timing analysis method (Michael et al., 2016), which provides an exact evaluation of the chronology model for the observed set of crater diameters. It differs from previous binning and curve-fitting analyses in that no approximations are used, and the absence of craters in some size ranges (previously "empty bins") is given proper consideration. The result is a probability function describing the likelihood of the unit having a given model age, which simultaneously describes the range of uncertainty of that value. For analyses including many crater measurements, the results are practically identical to previous methods. For those including only a small number of craters, the Poisson method yields significantly more accurate results and should always be preferred. Model ages are presented with an intrinsic function μ, which represents the unknown uncertainty of calibration of the chronology model that is not included in the Poisson probability function (Michael et al., 2016).

When using CTX images, we did not include craters smaller than 60 m in diameter. This minimum diameter of 60 m corresponds to approximately ten pixels of a CTX image, a limit chosen to reduce the potential bias in distinguishing a crater from a circular feature with no impact-related origin. When using HiRISE images our minimum limit was set to 15 m, constrained by the range of validity of the production function. In the case of the smaller deposits, the low counting area and the corresponding uncertainties of absolute model ages have to be considered in the further interpretation of the results. The epoch boundaries are based on the Neukum system (Hartmann & Neukum, 2001) as explained in Michael (2013).

3. Results

3.1. Geomorphological Observation

Several deposits on the flat floor of a S-N trending valley system south of Ariadnes Colles are characterized by (1) widths and lengths of a few kilometers (Figures 2–5), (2) convex upward surface topography (Figure 5), and (3) crevasses and fractures on their surfaces (Figures 2–4). They are referred to, in this study, as VFD. A total of 38 VFD have been observed and mapped in the study area; their location and surface areas (a few square kilometers to a few tens of square kilometers) are listed in Table 1. In the map of the distribution of major glacial ice deposits in the midlatitudes by Levy et al. (2014; Figure 1a) there are several CCF indicated in our study area (filled pink polygons in Figure 1b), but the VFD remained unreported. The host valley system floors, as well as areas surrounding the VFD, are partly covered by a thin mantle that appears to have a relatively smooth texture at HiRISE scale. This mantle is superposed by only very few impact craters smaller than a few meters, indicating a recent formation.

The VFD and the host valley system are partly situated within the extent of the ejecta blanket of the Tarq impact crater (Figure 1b). The ejecta blanket can be traced onto the floor of the valley system and the adjacent western plateau; however on the eastern side of the valley system the ejecta blanket is significantly less well developed (Figure 1b). The entire visible and mapped ejecta blanket covers an area of ~1.4×10^4 km^2. Tarq is a central-pit crater where the pit is ~4 km in diameter and located within the central peak. The VFD host valley system is situated approximately 75 km eastward from the center of Tarq crater. The main trunks of the host valley system are joined by narrow tributary channels. Adeli et al. (2016) suggested that these valleys are of fluvial origin and were fed by occasional surface runoff due to precipitation and ice/snow melt during the Early to Middle Amazonian.

Several VFD fill the entire width of their host valley (Figures 2 and 4), and some others are exposed in the center of the valley (Figures 3, 5, and 6a) from beneath the currently degrading thin mantle. In most

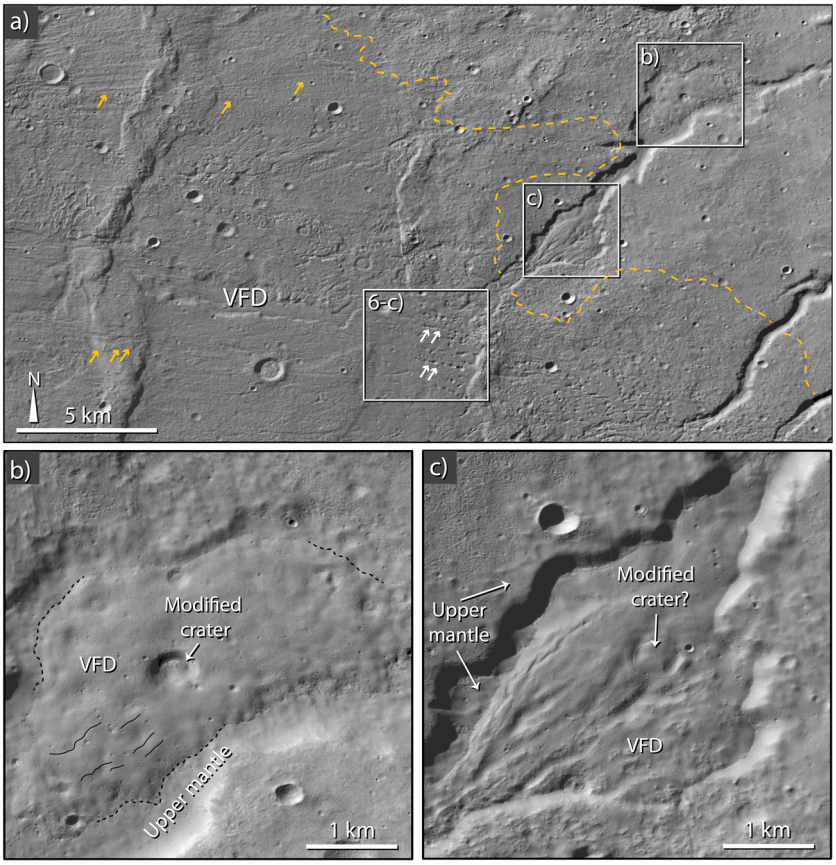

Figure 2. Valley fill deposits (VFD) distribution in the study area. (a) The VFD has almost filled entirely the host valley. The valley is a part of a fluvial system located in Terra Cimmeria. The orange dashed line represents the limit of visible ejecta blanket. The orange-colored arrows point to ejecta streaks. (b) VFD with a modified impact crater on its surface. The dashed black line represents the limit between the upper mantle and VFD. The solid line shows some crevasses. (c) VFD with longitudinal furrows. Note the marked circular feature which may represent a filled impact crater, and the adjacent small unmodified and fresh impact crater. Locations of (a) is shown in Figure 1b. All three figures show detail of Context Camera image B21_017798_1416.

cases, the areas surrounding the VFD are covered by either mantle and/or ejecta, where there is no observational window to the potential underlying material. Nevertheless, it is likely that the VFD entirely cover the floor of the host valley and have subsequently been partly covered by the ejecta and/or the thin mantle. In the case of one VFD (ID 2 in Table 1), higher resolution images and topographic data are available and it was possible to measure its dimensions (Figure 5). This deposit occurs in a ~3,000-m-wide valley and is ~1,800 m wide and 2,200 m in length. It ranges in height between ~30 and 40 m measured from the visible valley floor which is covered by the thin upper mantle (Figure 5).

On the surface of VFD we observe numerous crevasses and fractures (Figures 3b and 3c). At HiRISE scale we observe that the crevasses are continuous and connected to each other (Figures 3b and 3c) forming a wider network expanding across the entire VFD. They are mainly longitudinal, that is, parallel to the valley long axis. The widest longitudinal crevasses are a few meters (<10 m) in width and are interconnected by narrower transverse crevasses. The VFD in Figure 2c shows a more degraded and modified surface than most other VFD in this area. In the southwestern part of this VFD, some linear features and fractures are wider than the crevasses. There is also a circular feature, which may be an impact crater that is almost fully filled and covered but is still recognizable due to a concentric pattern of crevasses on the surface. Other circular fracture patterns are observed on a few other VFD (e.g., Figures 2b and 3b) and possibly represent the plan view outlines at the surface of buried impact craters. On the surfaces of all VFD, there are only a few impact craters with diameters equal to or smaller than ~700 m (Figures 2b and 3b) which are mostly degraded; their rims show almost no positive relief, and they have flat floors (at CTX resolution). There are also a few

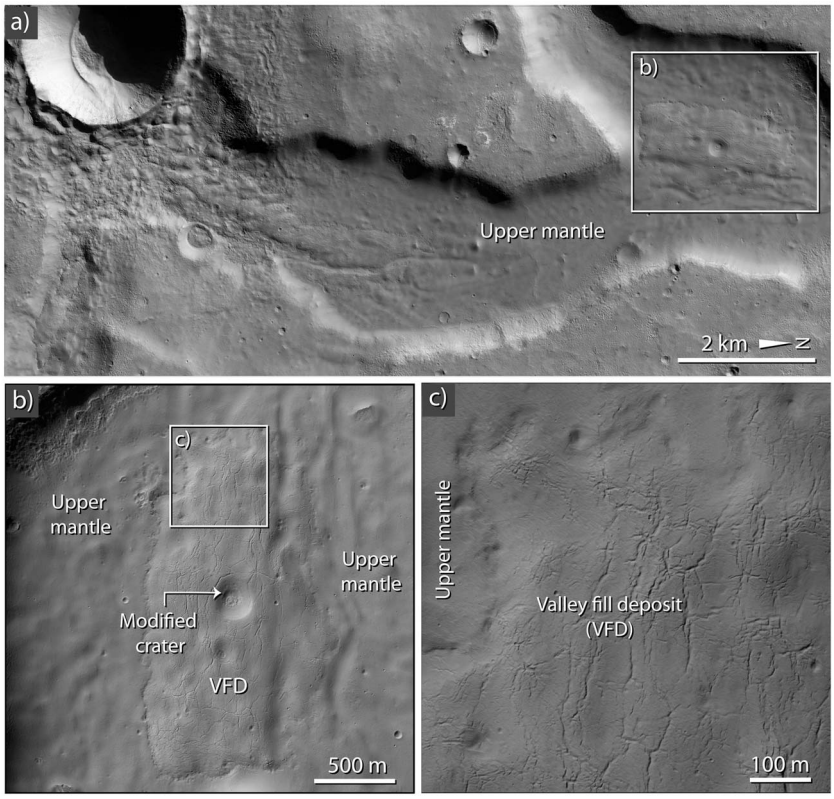

Figure 3. Valley fill deposits (VFD). (a) VFD observed in the center of the valley width, exposed beneath the upper mantle. The valley floor is partly covered by the VFD and partly by the upper mantle. (b) VFD with clear crevasses on its surface, and a modified impact crater. (c) A blow-up on the surface of the VFD in (b). The thin upper mantle was deposited on top of the VFD. Location of the (a) is indicated in Figure 1b. All three figures show details of HiRISE image ESP 016664_1420.

relatively small and undegraded impact craters (<60 m in diameter; Figure 2c), which do not show any modification of their rim and wall. In this area, the thin mantle is stratigraphically above the VFD and covers the valley floor and partly the VFD. Exemplary contacts between the thin mantle and the VFD are shown in Figures 3b and 3c.

On the floor of two valleys, we observe several kilometer-long VFD which locally fill the width and depth of the host valley system (Figure 4a). There is less ubiquitous mantle coverage in this area: As a consequence we can observe the contact between the VDF and the valley floor (at the beginning and end of each deposit along the valley). The VFD have several longitudinal crevasses on the surface and transverse crevasses at their long-valley margin (Figures 4b–4d). In the area adjacent to the VFD in both valleys, the valley floor has a rougher texture compared to the smoother texture of the VFD (Figures 4b and 4c). This may be caused by hummocky accumulations of sediment close to the VFD. The outcrops of rough material decrease gradually toward the north (i.e., away from the VFD) until the smoother valley floor is visible (Figures 4b and 4c). The area of this rough terrain extends around 1–3 km from the VFD in both valleys. At the contact between the VFD and valley walls we observe several rimless pits with diameters of a few tens of meters aligned along the border of the VFD (Figures 4c and 4d).

The VFD are mainly located within the visible and mapped boundary of the Tarq ejecta blanket (Figure 1b). The ejecta streaks are clearly observable in the vicinity of most of the VFD (Figures 2a and 4a) and in few cases on the surface of the VFD (Figure 4b). It appears that the ejecta streaks are covered by a thin and smooth mantle (Figures 6b and 6c). In several places we observe the traces of the ejecta partly covered by the mantle and partly uncovered. Figure 6c shows an example where the yellow arrows point to covered ejecta streaks and white arrows to uncovered ejecta. Where the ejecta streaks are uncovered, we observe pit-like structures which may indicate the removal of the upper mantle by sublimation (Figure 6c).

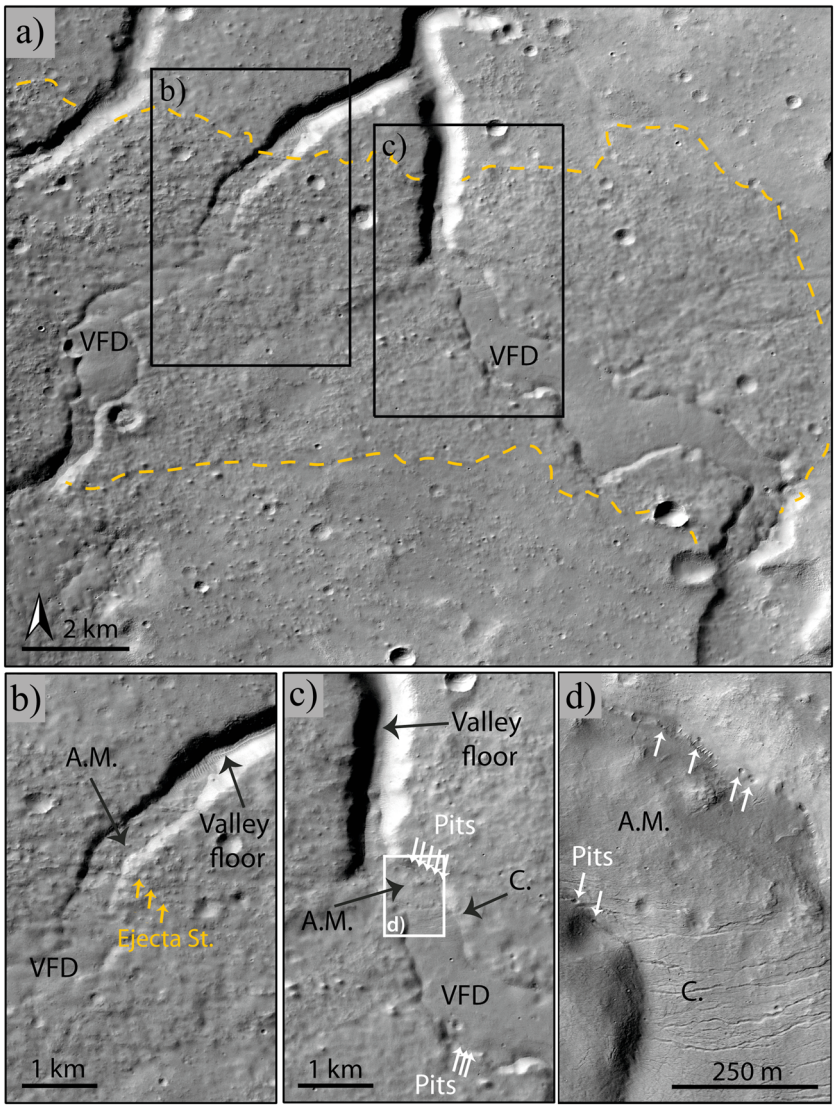

Figure 4. (a) Two VFD filling entirely the host valley system. (b and c) Blow-ups of the head of the glacier, showing the transverse crevasses (C.), the ablation moraine (A.M.), the valley floor, the ejecta streaks (Ejecta St. as yellow arrows), and the sublimation pits (white arrows). (d) Several pits on the border of the VFD. Location of (a) is shown in Figure 1b. All four figures show details of Context Camera image B18_016664_1414.

On the slope of the exterior wall of Tarq crater, we observe several narrow and isolated valleys with a simple morphology (Figures 6a and 6b). They have no tributaries and in some cases are joined by narrow valleys. These simple and narrow valleys are spatially isolated and locally display a sinuous plan view trace. These valleys typically originate at a given point without a visible depression (at CTX scale) and terminate at an unconfined area. We have not observed any depositional features such as alluvial fans that could be related to these narrow valleys. Some narrow valleys have been observed adjacent to VFD (Figure 6a), but they are much narrower than the VFD. These narrow valleys are different from the extended valley system which hosts the VFD.

3.2. Crater Size-Frequency Distribution

To constrain the formation age of the VFD, we measured the CSFD on the ejecta blanket of Tarq crater (Figure 7a). Then, we selected one VFD and the adjacent thin mantle, covered by HiRISE images (Figure 7b), in order to estimate their model ages. The uncertainties to derive a robust absolute model age for these deposits are due to (1) the surface of the VFD showing traces of resurfacing phase(s),

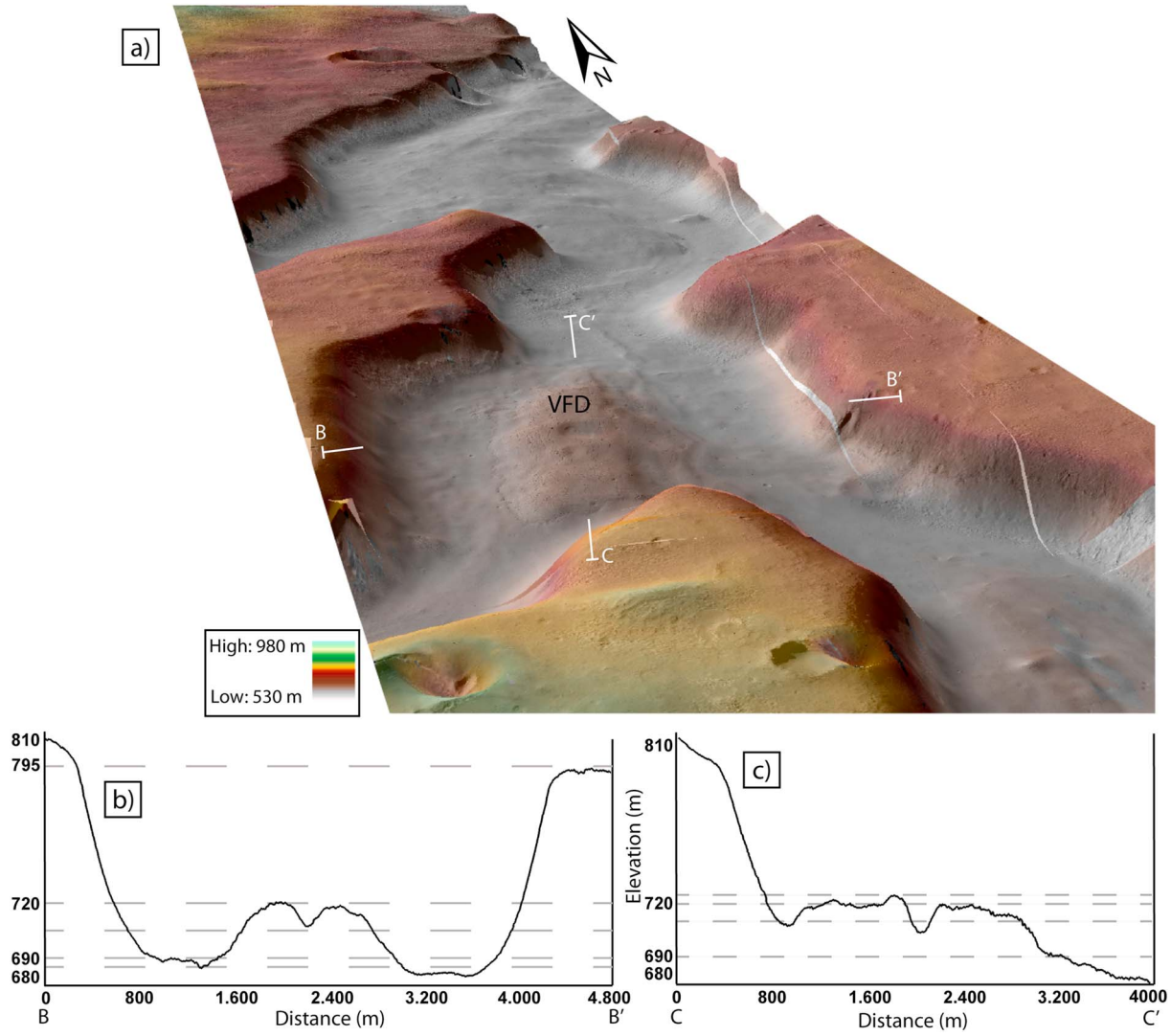

Figure 5. (a) HiRISE DEM of a valley fill deposit and its host valley, generated from two images of ESP_016664_1420 and ESP_045305_1420. Cross sections corresponding (b) to BB′ line in (a), and (c) to CC′ line in (a). The (b) and (c) cross sections show an example of VFD morphology and dimension, as well as that of the host valley.

such that craters may have been degraded and their morphology modified and (2) the low number of craters larger than 60 m on the surface of the VFD. The counting area of the ejecta blanket of Tarq crater, covered by CTX images (Figure 7a), was mapped conservatively in that the CSFD was measured on the inner part of the ejecta blanket, where its presence could be unambiguously identified. The outer part of the ejecta blanket appears to be thin, and thus distinguishing between pre-Tarq-impact and post-Tarq-impact event craters would be difficult. Fitting our crater distribution curve with Mars crater production function shows two model ages of μ410 (±50) Ma and μ3.6 (+0.1/−0.4) Ga (Figure 7c). The result shows clearly that at ~μ410 Ma (Middle Amazonian) this area has been resurfaced; thus, one of the following scenarios may hold:

I) The resurfacing event may have been the emplacement of the Tarq ejecta blanket, and therefore the impact occurred at ~μ410 Ma (Middle Amazonian).
II) The Tarq impact occurred at ~μ3.6 Ga (Late Hesperian), and the resurfacing age (~μ410 Ma) may be related to various resurfacing mechanisms such as the event which resulted in deposition and formation of VFD.

Table 1
All the Valley Fill Deposits (VFD) Mapped in This Study

ID	Coordinates		Area (km^2)	Shown in this study
	Lat	Lon		
1	−37.62	172.92	66.70	
2	−37.92	172.85	2.63	Figures 3a, 3b, 5a, and 7b
3	−38.02	172.89	4.34	
4	−38.07	172.92	0.74	
5	−38.15	172.78	3.16	
6	−38.36	172.82	7.79	Figure 4a
7	−38.34	172.67	3.89	Figure 4a
8	−38.41	172.64	3.67	
9	−38.43	172.62	4.98	
10	−38.66	172.59	1.10	
11	−38.69	172.61	1.63	
12	−38.39	172.52	10.65	
13	−38.39	172.46	22.29	
14	−38.13	172.52	8.25	Figures 2a and 2c
15	−38.01	172.62	8.69	Figures 2a and 2b
16	−37.94	172.51	9.34	
17	−37.93	172.44	1.44	
18	−37.88	172.54	2.45	
19	−37.81	172.57	2.01	
20	−37.79	172.56	1.92	
21	−37.79	172.54	1.66	
22	−37.75	172.61	0.76	
23	−37.71	172.53	3.05	
24	−37.64	172.51	1.43	Figure 6a
25	−37.40	172.27	16.80	
26	−37.59	172.37	1.16	
27	−37.63	172.32	6.51	Figure 6a
28	−37.70	172.31	4.82	
29	−37.75	172.37	0.55	
30	−37.62	172.20	5.05	
31	−37.62	172.10	16.07	
32	−37.80	172.23	1.44	
33	−38.18	172.26	7.90	
34	−38.88	172.03	46.05	
35	−38.90	171.91	19.83	
36	−39.04	171.86	0.73	
37	−39.13	171.87	5.01	
38	−39.36	171.59	79.27	Figure S1

An impact event resulting in a crater with a similar diameter as Tarq (~35 km) occurs on Mars with the present impact rate roughly once per 15 Ma (see Figure 2 in Hartmann & Daubar, 2017). This means approximately 27 impact craters of ~35-km diameter formed in the past 410 Ma over the whole planet. This small number makes it less likely that Tarq formed within this period. Therefore, we need to combine this result with geomorphological evidence of the impact crater morphology and its ejecta blanket, in order to constrain the most likely absolute model age of Tarq crater (see section 4.2.).

In order to estimate the absolute model age of the VFD, we chose one deposit covered by a HiRISE image (Figure 7b). The counting area is similar to the mapped surface of the VFD. The unit/counting area limit was mapped along the visible boundary of the encompassing mantle. The VFD has an area of ~2.04 km^2 within which a total of 46 impact craters were counted. The CSFD curve (Figure 7d) shows a μ21 (+10/−8) Ma model age corresponding to the VFD and to the Late Amazonian epoch. The youngest age of μ3.7 (±2) Ma most likely relates to the recent emplacement of the thin upper mantle in this area and is in agreement with the model age derived from the surface of the mantle of μ3.5 (+2/−1) Ma (Figure 7e). The age of μ17 (+10/−8) Ma could also be consistent with the VFD surface model age. We therefore interpret that the VFD may have formed during the Late Amazonian.

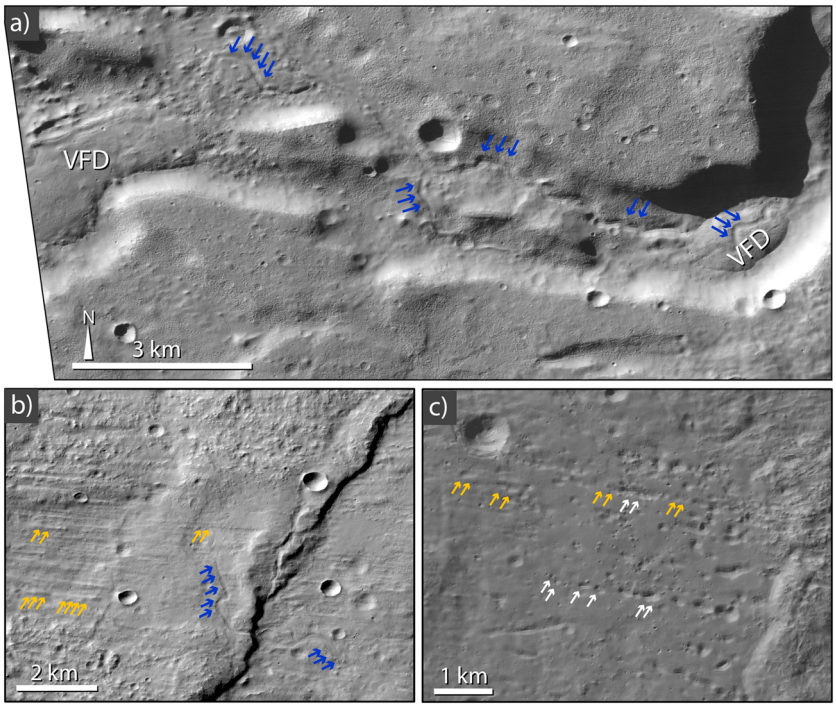

Figure 6. (a) Narrow and simple valleys adjacent to VFD shown by blue arrows. Two small VFD are also marked. Detail of CTX image B21_017798_1416. (b) The ejecta streak shown by yellow arrows and narrow fluvial valleys adjacent to the ejecta blanket shown by blue arrows. Detail of CTX image P16_007434_1416. (c) Ejecta streaks covered by a thin upper mantle (yellow arrows) and uncovered (white arrows). Detail of CTX image B20_017442_1433. Location of (a) and (b) are shown in Figure 1b, and location of (c) in Figure 2a.

4. Discussion

4.1. Origin of the VFD

The VFD have been observed on the floors of a valley system which displays evidence of Early to Middle Amazonian fluvial activity (Adeli et al., 2016). This host valley system is located approximately 75 km eastward from the Tarq central pit crater (Figure 1b). The VFD fill the host valley floor to various degrees (partly or fully) in different sections and have a convex-upward morphology; these characteristics indicate a post-valley deposition of VFD. The host valley floor as well as VFD and the areas surrounding the VFD are partly covered by a thin, smooth-textured mantle. This mantle is superposed by a very few and small ($\leq$ a few meters) impact craters, indicating a recent formation. This thin mantle may correspond to the latitude-dependent mantle (LDM) that covers large parts of the mid- and high latitudes in both hemispheres (Kostama et al., 2006; Mustard et al., 2001).

On the surface of few VFD, where an absence of the upper mantle enables observing the entire VFD surface, we observe widespread longitudinal and traverse fractures. Longitudinal fractures are oriented parallel to the valley axis and thus to the flow direction, indicating some lateral extension of the deposits. The transverse fractures (C. in Figures 4c and 4d) resemble crevasses on terrestrial glaciers and may have formed due to the flow of ice and its brittle deformation. In this case the principle stress would be parallel to the direction of the ice movement, so that transverse crevasses open up at right angles to the center line and curve downstream by the drag of the valley walls (Benn & Evans, 2010). Alternatively, the crevasses could have formed due to lateral and vertical variations of the flow velocity vector field between the base and top of the VFD or by volume loss due to sublimation of ice. In the latter case, the ice deposit would gradually taper out down-valley without a significant movement or flow along the valley. The circular crevasses observed on several VFD, tracing the outline of buried impact craters (Figures 2b and 3b), may indicate collapse as a consequence of volume loss due to ice sublimation. In addition, the circular shape of these impact craters points toward loss of volume rather than an along-valley viscous flow, in which case they would be

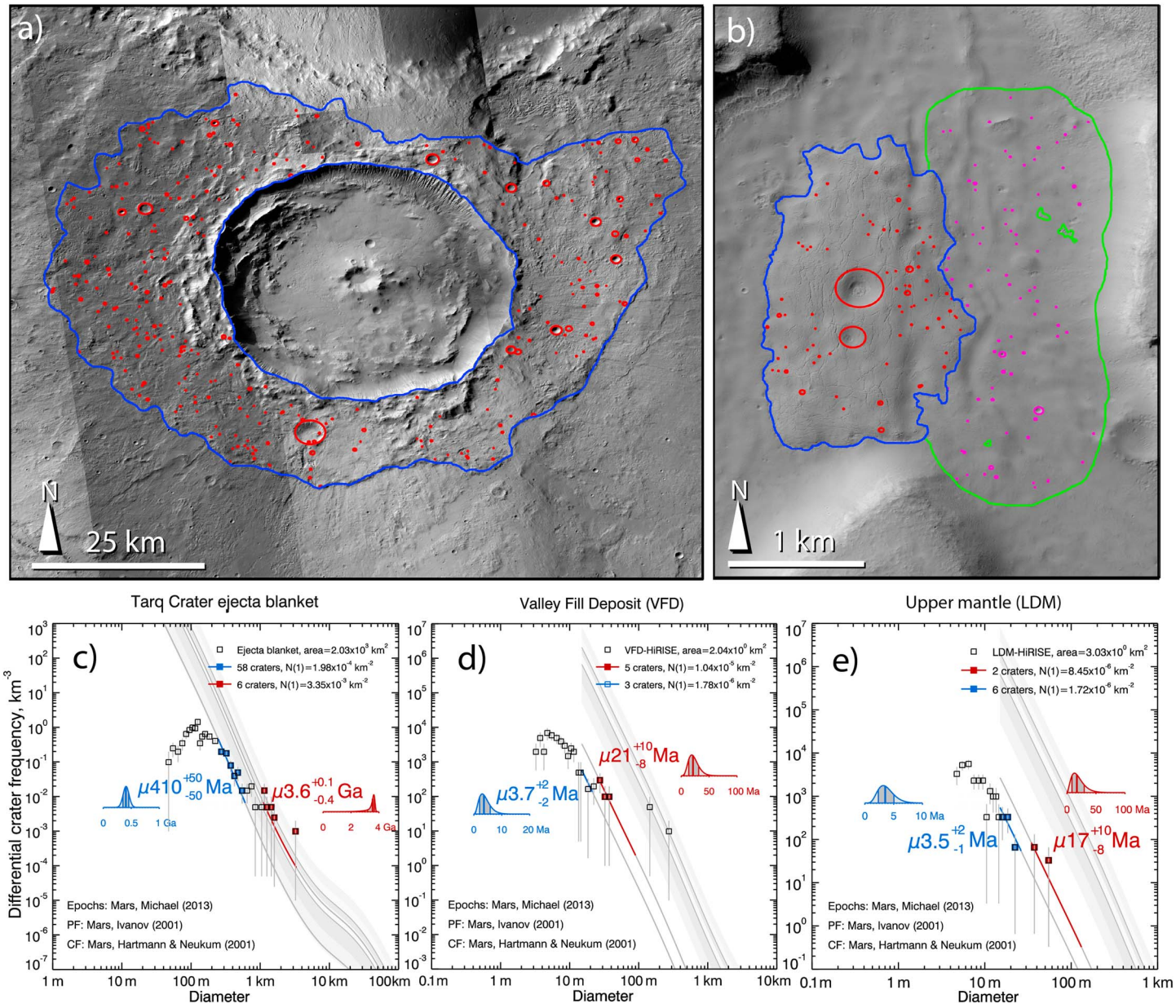

Figure 7. Absolute model ages (a) crater counting area of Tarq crater on a mosaic of Context Camera images (G16_024378_1409; B19_016941_1416; P15_006933_1393; P18_007935_1401; P11_005298_1418; P16_007434_1416; G12_022967_1431). (b) one valley fill deposit and its adjacent upper mantle (LDM; HiRISE image ESP 016664_1420). (c) The absolute model age corresponding to the ejecta blanket (a), (d) the valley fill deposit (b), and (e) the upper mantle (b). The μ is a function representing the uncertainty of calibration of the chronology model (Michael et al., 2016).

expected to have a distorted (i.e., elliptical) plan view shape. The accumulated sediments at the head of the VFD have a rough surface texture and a different morphology as compared to the smooth VFD surface. In an ice deposit scenario, these sediments may represent remnant deposits from glacier retreat by ice sublimation, known as ablation moraines (A.M. in Figures 4b and 4c). The rimless pits aligned at the margin of some VFD and the valley wall (Figures 4c and 4d) indicate volume loss by sublimation and collapse, further supporting the notion of a substantial amount of ice in the VFD. Pits possibly due to ice sublimation have often been observed at midlatitude ice-related landforms (Mangold, 2003; Mangold, 2011). The combined observation of transverse crevasses, ablation moraines, and sublimation pits suggests that the sublimation at the ice deposit front caused the deposit surface to collapse locally, inducing tensile stress and the opening of the crevasses.

In an ice deposit scenario, the VFD would be small-scale debris-covered stagnant ice deposits located on the floors of a valley system. The crevasses and sublimation pits indicate that they are in a degradational phase. Thus, the current VFD are remnants of larger ice deposits. At this stage we are unable to estimate how much larger the initial deposit(s) were or how long the degradation has taken. In any case, the VFD have been preserved in the Martian climate until today. This preservation may most likely be due to (1) the protective effect of an upper, supraglacial layer of debris and dust lag (Baker & Carter, 2019) and (2) the protective effect of the valley topography, which would act as a sink for airborne dust deposits. The role of the valley morphology in the preservation of the VFD appears important, because we can only observe the VFD in the valley system and not the plateau around. Therefore, we suggest that the valley topography helped to protect and to preserve the ice deposit of VFD, which are also covered by a lag layer. The thickness of the lag layer and the ice content of the VFD are unknown. There is no observational evidence which would enable favoring either a "dirty" ice with a high ratio of debris and dust to ice or an almost pure ice covered by a dust lag.

Besides the above described evidence of the icy nature of the VFD, the Tarq impact crater and its ejecta blanket also reveal an ice-related landscape. On the ejecta blanket, there are traces of local melting events, observed as simple and narrow fluvial valleys (Figures 6a and 6b). These valleys are comparable with glacio-fluvial valleys reported previously as a result of the melting of shallow ice below warm ejecta (Grant & Wilson, 2018; Mangold, 2012) and were mostly observed on the ejecta blanket of craters dated as the Late Hesperian to the Middle Amazonian (Mangold, 2012). Moreover, Tarq crater has a central pit with raised rims (Figure 7a) which is indicative of an explosive origin by impact into an icy substrate (Williams et al., 2015).

The lineated valley fill (LVF) is interpreted to be a type of terrain on the floor of valleys, mainly in the so-called Fretted Terrain at the dichotomy boundary (e.g., Head et al., 2006, 2010, Squyres, 1978, 1979, Squyres & Carr, 1986). LVF may be analogous to debris-covered glaciers due to its similarity to terrestrial valley glaciers, including crevasses and lateral and medial moraines (see, e.g., Head et al., 2006). Radar observations showed that LVF and related deposits such as lobate debris aprons (LDA) and concentric crater fill (CCF) (Squyres, 1978, 1979; Squyres & Carr, 1986) contain a core of relatively pure water ice (Holt et al., 2008; Plaut et al., 2009). Although there are similarities between LVF and VFD, some differences suggest they may not have formed in the same way. The LVF belongs, together with LDA and CCF, to a major group of large-scale glacial landforms which is believed to have formed during the Middle to Late Amazonian (e.g., Head et al., 2010). The major criteria to identify LVF as described by Head et al. (2010) are (1) alcove, theater-shaped indentations in a valley, (2) parallel arcuate ridges facing outward from the alcoves and extending downslope as lobe-like features, and (3) shallow depressions between the ridges. None of these have been observed in VFD. We did observe crevasses, but they are far smaller in scale than the typical ridges observed on the LVF surface. Therefore, we suggest that the VFD reported in this study are small-scale ice deposits of a most likely different morphological type than the LVF/LDA/CCF family and other large-scale debris-covered glaciers.

We also analyzed the alternative hypothesis that VFD were accumulated through the deposition of fluvial or aeolian sediments. In the case of fluvial sediments, however, we would not observe the deposits filling the entire depth of the host valley, as is the case at some places in this study (e.g., Figures 2a and 4a). Therefore, given the post-depositional deformation record of the VFD, and their almost complete infilling of the host valley, it is unlikely that VFD represent sediments transported and deposited by fluvial processes. In the case of aeolian activity, the valley may have provided a sink for sediments carried by wind (Bourke et al., 2004), which could result in localized sediment deposition. We would, however, then expect to observe similar deposits in other depressions in this area as well as in other valleys in the neighboring regions. In contrast, the local distribution of VFD on the eastern side of Tarq crater and its restriction to the host valley system does not support a widespread emplacement of material and therefore does not suggest an aeolian origin for VFD.

Combining all our geomorphological observations indicates that the bulk of the VFD contains material rich in ice. These observations are (1) the concave-upward morphology of VFD, (2) the occasional complete infilling of the host valley, (3) the presence of longitudinal and traverse crevasses, (4) local collapse features on their surface, and (5) the presence of sublimation pits. In addition, there is independent evidence of the presence of ice in the study area. This evidence consists of (1) a central pit within the Tarq crater, which may

Table 2
The VFD Formation Scenarios (See Section 4.2)

Scenario	Impact age	VFD emplacement age	VFD emplacement mechanism	Consistent observations	Inconsistent observations
I	Middle Amazonian	Middle Amazonian	Impact into icy strata	Ejecta blanket overlaying the VFD and surrounding area (Figures 2a and 4a) Glacio-fluvial valleys on the ejecta blanket (Figures 6a and 6b) Pitted central peak of Tarq crater (Figures 1a and 7)	Crater size-frequency distribution (Figure 7)
II	Late Hesperian or Middle Amazonian	Middle Amazonian or Late Amazonian	Precipitation	Crater size-frequency distribution (Figure 7)	Ejecta blanket overlaying the VFD and surrounding area (Figures 2a and 4a) Local distribution of VFD (Figure 1b)

reveal an impact into a subsurface layer of ice and (2) glacio-fluvial valleys on the ejecta blanket, which may point to the melting of shallow subsurface ice due to the emplacement of the ejecta.

4.2. The VFD Formation Mechanism

The current distribution of the VFD is restricted to the topographically low regions of the fluvial valley system. This suggests that the valley topography may have enabled either the deposition of a thicker reservoir of ice than on the adjacent plains or the preferential preservation of ice inside the valley due to slower sublimation and formation of a thicker sublimation lag, or both. The VFD are observed within the extent of the Tarq crater ejecta blanket, and the ejecta streaks were observed in the vicinity of VFD (Figures 1b, 2a, and 4a) and in some cases on their surface (Figure 4a and b). This suggests that the impact crater formation and the ejecta emplacement may have played a role in the formation and/or preservation of VFD. Nonetheless, the formation mechanism resulting in the deposition and/or distribution of the VFD appears to be less clear. The geomorphological observations suggest a link between the ejecta blanket of Tarq crater and the VFD. However, the crater size-frequency distribution (CSFD) of Tarq crater (see section 3.2.) raises the question of whether Tarq crater was formed in the Late Hesperian or Middle Amazonian and also whether the VFD emplacement took place in the Middle Amazonian or in the Late Amazonian. Thus, from the CSFD results it is unclear whether the VFD and the ejected material were emplaced at the same time during the Middle Amazonian or the VFD formation is due to a post-impact event. In the following, we examine these two possible scenarios (Table 2) for the formation, distribution, and preservation of VFD based on our geomorphological observations and the absolute model age estimation.

4.2.1. Scenario I: Impact Into an Icy Stratum During Middle Amazonian

There are various lines of evidence for both glacial and excess ice in the midlatitudes of Mars (e.g.Bramson et al., 2017, Dundas et al., 2018, Kadish & Head, 2011, Levy et al., 2014, Stuurman et al., 2016, Viola & McEwen, 2018), both at present and in the past. Modeling the impact of a projectile into an icy stratum under Martian conditions shows that the formation of a midsized impact crater (30–50 km in diameter) results in the origin of a hot water-bearing central uplift with mean temperatures in the periphery generally remaining below the melting point of water (Ivanov & Pierazzo, 2011; Pierazzo et al., 2005; Senft & Stewart, 2008; Sherburn & Horstemeyer, 2010). Pierazzo et al. (2005) and Ivanov and Pierazzo (2011) modeled the post-impact thermal state of a layer of mixed rock and water ice, under Martian conditions. Senft and Stewart (2008) modeled impacts into a near-surface ice layer and show that the impact results in the distribution of ice on the surface, which may be covered by a layer of ejected material. In addition, models analyzing the ejecta emplacement on a layer of subsurface ice (Weiss & Head, 2016) conclude that the postimpact temperature of the ejecta emplaced on ice, and therefore contact melting, occurs as a function of ejecta thickness and radial distance from the crater rim crest. On the Tarq crater ejecta blanket adjacent to the crater rim, we observed narrow channels (Figure 6a), which indicates local melting events. The VFD, however, are located a few tens of kilometers away from the impact crater (Figure 1b), where the ejecta blanket coverage has a less visible presence; therefore, where we observe VFD, the contact melting has most likely not taken place. The observation of a pit with raised rims in the center of Tarq crater (Figure 7a) suggests that the impact event

most probably occurred in the presence of a layer of subsurface ice (Williams et al., 2015). The stratigraphy of the ejecta blanket on top of the VFD and their surrounding area further suggests that the VFD emplacement is closely linked to the emplacement of the ejecta blanket.

As described above, the CSFD of the ejecta blanket shows two possible model ages for the Tarq crater formation. In scenario I, we assume that an impact in the Middle Amazonian in an icy substrate resulted in the distribution of ice over a broad area. Materials deposited on the floor of the host valley system were preserved as stagnant ice deposits covered by a wind-blown protective lag layer due to the low topography of the valley system. Ice deposited on the plateau outside of this valley system has subsequently been sublimated. The only observation inconsistent with this scenario is the Late Amazonian model age of the VFD (Figure 7d). This could likely be the approximate time window of the last major ice deposition and modification in the midlatitudes, and thus, the surface could have been covered and/or modified by these events. It is also important to note that this model age is based on very few craters. Hence, scenario I is consistent with our geomorphological observations but inconsistent with our estimated model ages (Table 2).

4.2.2. Scenario II: Post-impact Ice Emplacement During Middle or Late Amazonian

In scenario II, we assume that the VFD emplacement took place after and independently of the impact event. Here, the impact could have occurred either in the Late Hesperian or in the Middle Amazonian. In both cases the VFD were emplaced post-impact, either in the Middle Amazonian or in the Late Amazonian (see section 3.2. for the model ages). The widespread presence of large-scale debris-covered glaciers in the midlatitudes during the Middle to Late Amazonian has been documented in various studies (e.g.Head et al., 2005, Levy et al., 2014). Therefore, we may assume that ice had also been deposited in the study area via precipitation. This would result in a widespread distribution of ice-related material in this region. However, we have not observed any other similar ice deposits in the surrounding area of the valley system. As in scenario I, we may assume that ice deposited in the valleys has been preserved, whereas ice deposited outside the valley has been sublimated. In any case, the ejecta blanket within the region of the valley system would have been covered by these deposits, which appears not to be the case. Although a very thin layer of ice has been observed partly covering the ejecta (e.g., Figures 6b and 6c), this layer is most likely a very late emplacement, which is degrading under the current conditions. The scenario II of post-impact ice emplacement in this area, therefore, is not consistent with our geomorphological observations (Table 2).

5. Conclusions and Implications

Several lines of evidence hint at the presence of debris-covered glaciers in the midlatitude regions of Mars (Head & Marchant, 2003; Holt et al., 2008; Plaut et al., 2009; Levy et al., 2014; Figure 1a). While they display diverse morphological characteristics, they all show common features pointing to their glacial nature. Here, we present evidence of stagnant ice deposits (referred to as VFD) observed locally inside a valley system in the Terra Cimmeria region. Our observations of the VFD enable us to analyze their origin with implications for the Amazonian regional climate.

The VFD were observed within the limits of the ejecta blanket of the Tarq impact crater, the ejecta streaks of which are partly covering the areas surrounding the VFD as well as the surface of a few VFD. The central pit of this impact crater points to a potential impact into an ice-bearing substrate. The presence of glacio-fluvial valleys further supports this notion. Our geomorphological observations indicate that the VFD are small-scale debris-covered stagnant ice deposits and are currently in degradational stage. These observations include the following: (1) the convex-upward morphology, (2) the infilling, in some cases, of the entire valley depth, (3) crevasses on their surface, and in some cases traces of volume loss of the deposit, and (4) sublimation pits. The local distribution of the VFD and their stratigraphic relation to the ejecta blanket, combined with the evidence of the Tarq impact crater having been formed in an ice-bearing substrate, suggest that the distribution and thus formation of VFD may be linked with the Tarq impact event. Our crater size-frequency distribution results, however, show two major resurfacing events in the area and therefore two possible formation times for the Tarq crater: Late Hesperian or Middle Amazonian. In order to clearly address this ambiguity, we described two plausible scenarios for the emplacement of the VFD (Table 2):

Scenario I The Tarq impact took place during the Middle Amazonian, into an icy target substrate. Impact into subsurface ice should result in a mixture of ejected solid particles and water ice distributed over the impact crater periphery. The material deposited on the floor of the host valley system

has then been preferentially protected against sublimation by a wind-blown lag deposited in the topographic lows of the valley system, covering the VFD. This scenario fits our geomorphological observation but can hardly be explained by the model age estimation (Table 2).

Scenario II The Tarq impact took place either during the Late Hesperian or Middle Amazonian. After the impact, the VFD were emplaced in this area by precipitation as a widespread surficial ice layer, which was later modified and degraded. This may have happened similarly to the formation of the large-scale debris-covered glaciers (e.g., LVF and LDA). In this case, we would expect the deposit to have a less localized distribution and more importantly to cover the ejecta blanket of Tarq crater. This is, however, not the case as some ejecta streaks are on top of the VFD. This scenario, although inconsistent with most of our geomorphological observations, would however be consistent with the estimated model ages (Table 2).

In both scenarios the host valley topography is essential in preserving the ice deposits of VFD. We favor scenario I—VFD distribution due to impact into an icy substrate—because it is consistent with all of our geomorphological observations. VFD are debris-covered stagnant ice deposits with a likely age of Middle Amazonian, which were not reported in the previous studies (such as in the map of Levy et al., 2014; Figure 1). These deposits have been preserved most likely due to a lag of dust and debris deposited in the valley's topographic lows and are currently in a degradational phase. They highlight the importance of local geologic conditions (i.e., impact into icy strata; ice emplacement in topographic lows) for the current distribution of ice deposits on the surface of Mars. Although the VFD have a local presence, they hint to a likely possibility of presence of various and more widespread buried ice deposits in the midlatitudes, which require detailed investigations of high-resolution data. The buried ice deposits are important for better comprehending the climate during their emplacement, the preservation processes, and for the identification of special regions (Rettberg et al., 2016) for future human exploration and/or in situ resource utilization (Mungas et al., 2006; Wasilewski, 2018).

Acknowledgments
We would like to warmly thank Eric Petersen and two anonymous reviewers for their constructive comments and helpful feedback. The data that were used to prepare this paper were provided by the PDS Geosciences Node archive (http://pds-geosciences.wustl.edu/) and by the Planetary Science Archive (https://archives.esac.esa.int/psa/). The data presented as supporting information include SHARAD simulations (by I. B. S.) and detailed information related to crater counting results (by S. A. and G. G. M.).

References

Adeli, S., Hauber, E., Kleinhans, M., Le Deit, L., Platz, T., Fawdon, P., & Jaumann, R. (2016). Amazonian-aged fluvial system and associated ice-related features in Terra Cimmeria, Mars. *Icarus*, *277*, 286–299. https://doi.org/10.1016/j.icarus.2016.05.020

Baker, D. M. H., & Carter, L. M. (2019). Probing supraglacial debris on Mars 1: Sources, thickness, and stratigraphy. *Icarus*, *319*, 745–769. https://doi.org/10.1016/j.icarus.2018.09.001

Benn, D. I., & Evans, D. J. A. (2010). *Glaciers and glaciation* (p. 802). London: Hodder Education.

Berman, D. C., Crown, D. A., & Joseph, E. C. S. (2015). Formation and mantling ages of lobate debris aprons on Mars: Insights from categorized crater counts. *Planetary and Space Science*, *111*, 83–99. https://doi.org/10.1016/j.pss.2015.03.013

Bourke, M. C., Bullard, J. E., & Barnouin-Jha, O. S. (2004). Aeolian sediment transport pathways and aerodynamics at troughs on Mars. *Journal of Geophysical Research*, 109, E07005. https://doi.org/10.1029/2003JE002155

Bramson, A. M., Byrne, S., & Bapst, J. (2017). Preservation of midlatitude ice sheets on Mars. *Journal of Geophysical Research: Planets*, *122*, 2250–2266. https://doi.org/10.1002/2017JE005357

Byrne, S., Dundas, C. M., Kennedy, M. R., Mellon, M. T., McEwen, A. S., Cull, S. C., et al. (2009). Distribution of mid-latitude ground ice on Mars from new impact craters. *Science*, *325*(5948), 1674–1676. https://doi.org/10.1126/science.1175307

Cull, S., Arvidson, R. E., Mellon, M. T., Skemer, P., Shaw, A., & Morris, R. V. (2010). Compositions of subsurface ices at the Mars Phoenix landing site. *Geophysical Research Letters*, *37*, L24203. https://doi.org/10.1029/2010GL045372

Dickson, J. L., Head, J. W., & Marchant, D. R. (2008). Late Amazonian glaciation at the dichotomy boundary on Mars: Evidence for glacial thickness maxima and multiple glacial phases. *Geology*, *36*, 411–414. https://doi.org/10.1130/G24382A.1

Dundas, C. M., Bramson, A. M., Ojha, L., Wray, J. J., Mellon, M. T., Byrne, S., et al. (2018). Exposed subsurface ice sheets in the Martian mid-latitudes. *Science*, *359*(6372), 199–201. https://doi.org/10.1126/science.aao1619

Dundas, C. M., Byrne, S., McEwen, A. S., Mellon, M. T., Kennedy, M. R., Daubar, I. J., & Saper, L. (2014). HiRISE observations of new impact craters exposing Martian ground ice. *Journal of Geophysical Research: Planets*, *119*, 109–127. https://doi.org/10.1002/2013JE004482

Fassett, C. I., Levy, J. S., Dickson, J. L., & Head, J. W. (2014). An extended period of episodic northern mid-latitude glaciation on Mars during the Middle to Late Amazonian: Implications for long-term obliquity history. *Geology*, *42*(9), 763–766. https://doi.org/10.1130/G35798.1

Forget, F., Haberle, R. M., Montmessin, F., Levrard, B., & Head, J. W. (2006). Formation of glaciers on Mars by atmospheric precipitation at high obliquity. *Science*, *311*, 368–371. https://doi.org/10.1126/science.1120335

Grant, J. A., & Wilson, S. A. (2018). The nature and emplacement of distal aqueous-rich ejecta deposits from Hale crater, Mars. *Meteoritics & Planetary Science*, *53*(4), 839–856. https://doi.org/10.1111/maps.12843

Greve, R., Grieger, B., & Stenzel, O. J. (2010). MAIC-2, a latitudinal model for the Martian surface temperature, atmospheric water transport and surface glaciation. *Planetary and Space Science*, *58*(6), 931–940. https://doi.org/10.1016/j.pss.2010.03.002

Gwinner, K., Jaumann, R., Hauber, E., Hoffmann, H., Heipke, C., Oberst, J., et al. (2016). The High Resolution Stereo Camera (HRSC) of Mars Express and its approach to science analysis and mapping for Mars and its satellites. *Planetary and Space Science*, *126*, 93–138. https://doi.org/10.1016/j.pss.2016.02.014

Hartmann, W. K., & Daubar, I. J. (2017). Martian cratering 11. Utilizing decameter scale crater populations to study Martian history. *Meteoritics & Planetary Science*, *52*(3), 493–510. https://doi.org/10.1111/maps.12807

Hartmann, W. K., & Neukum, G. (2001). Cratering chronology and the evolution of Mars. *Space Science Reviews*, *96*(1), 165–194. https://doi.org/10.1023/a:1011945222010

Hauber, E., van Gasselt, S., Chapman, M. G., & Neukum, G. (2008). Geomorphic evidence for former lobate debris aprons at low latitudes on Mars: Indicators of the Martian paleoclimate. *Journal of Geophysical Research*, *113*, E02007. https://doi.org/10.1029/2007JE002897

Head, J. W., & Marchant, D. R. (2003). Cold-based mountain glaciers on Mars: Western Arsia Mons. *Geology*, *31*, 641–644. https://doi.org/10.1130/0091-7613(2003)031<0641:CMGOMW>2.0.CO;2

Head, J. W., Marchant, D. R., Agnew, M. C., Fassett, C. I., & Kreslavsky, M. A. (2006). Extensive valley glacier deposits in the northern mid-latitudes of Mars: Evidence for Late Amazonian obliquity-driven climate change. *Earth and Planetary Science Letters*, *241*(3-4), 663–671. https://doi.org/10.1016/j.epsl.2005.11.016

Head, J. W., Marchant, D. R., Dickson, J. L., Kress, A. M., & Baker, D. M. (2010). Northern mid-latitude glaciation in the Late Amazonian period of Mars: Criteria for the recognition of debris-covered glacier and valley glacier landsystem deposits. *Earth and Planetary Science Letters*, *294*(3–4), 306–320. https://doi.org/10.1016/j.epsl.2009.06.041

Head, J. W., Mustard, J. F., Kreslavsky, M. A., Milliken, R. E., & Marchant, D. R. (2003). Recent ice ages on Mars. *Nature*, *426*, 797–802. https://doi.org/10.1038/nature02114

Head, J. W., Neukum, G., Jaumann, R., Hiesinger, H., Hauber, E., Carr, M., et al. (2005). Tropical to mid-latitude snow and ice accumulation, flow and glaciation on Mars. *Nature*, *434*(7031), 346–351. https://doi.org/10.1038/nature03359

Holt, J. W., Safaeinili, A., Plaut, J. J., Head, J. W., Phillips, R. J., Seu, R., et al. (2008). Radar sounding evidence for buried glaciers in the southern mid-latitudes of Mars. *Science*, *322*(5905), 1235–1238. https://doi.org/10.1126/science.1164246

Hubbard, B., Souness, C., & Brough, S. (2014). Glacier-like forms on Mars. *The Cryosphere*, *8*(6), 2047–2061. https://doi.org/10.5194/tc-8-2047-2014

Ivanov, B. A. (2001). Mars/Moon cratering rate ratio estimates. *Space Science Reviews*, (96), 87–104.

Ivanov, B. A., & Pierazzo, E. (2011). Impact cratering in H_2O-bearing targets on Mars: Thermal field under craters as starting conditions for hydrothermal activity. *Meteoritics & Planetary Science*, *46*(4), 601–619. https://doi.org/10.1111/j.1945-5100.2011.01177.x

Jaumann, R., Neukum, G., Behnke, T., Duxbury, T. C., Eichentopf, K., Flohrer, J., et al. (2007). The High-Resolution Stereo Camera (HRSC) experiment on Mars Express: Instrument aspects and experiment conduct from interplanetary cruise through the nominal mission. *Planetary and Space Science*, *55*(7-8), 928–952. https://doi.org/10.1016/j.pss.2006.12.003

Kadish, S. J., & Head, J. W. (2011). Impacts into non-polar ice-rich paleodeposits on Mars: Excess ejecta craters, perched craters and pedestal craters as clues to Amazonian climate history. *Icarus*, *215*, 34–46. https://doi.org/10.1016/j.icarus.2011.07.014

Kirk, R. L., Howington-Kraus, E., Rosiek, M. R., Anderson, J. A., Archinal, B. A., Becker, K. J., et al. (2008). Ultrahigh resolution topographic mapping of Mars with MRO HiRISE stereo images: Meter-scale slopes of candidate Phoenix landing sites. *Journal of Geophysical Research*, *113*, E00A24. https://doi.org/10.1029/2007JE003000

Kneissl, T., van Gasselt, S., & Neukum, G. (2011). Map-projection-independent crater size-frequency determination in GIS environments—New software tool for ArcGIS. *Planetary and Space Science*, *59*, 1243–1254. https://doi.org/10.1016/j.pss.2010.03.015

Kostama, V.-P., Kreslavsky, M. A., & Head, J. W. (2006). Recent high-latitude icy mantle in the northern plains of Mars: Characteristics and ages of emplacement. *Geophysical Research Letters*, *33*, L11201. https://doi.org/10.1029/2006GL025946

Laskar, J., Correia, A. C. M., Gastineau, M., Joutel, F., Levrard, B., & Robutel, P. (2004). Long term evolution and chaotic diffusion of the insolation quantities of Mars. *Icarus*, *170*, 343–364. https://doi.org/10.1016/j.icarus.2004.04.005

Levrard, B., Forget, F., Montmessin, F., & Laskar, J. (2007). Recent formation and evolution of northern Martian polar layered deposits as inferred from a global climate model. *Journal of Geophysical Research*, *112*, E06012. https://doi.org/10.1029/2006je002772

Levy, J., Head, J. W., & Marchant, D. R. (2010). Concentric crater fill in the northern mid-latitudes of Mars: Formation processes and relationships to similar landforms of glacial origin. *Icarus*, *209*, 390–404. https://doi.org/10.1016/j.icarus.2010.03.036

Levy, J. S., Fassett, C. I., Head, J. W., Schwartz, C., & Watters, J. L. (2014). Sequestered glacial ice contribution to the global Martian water budget: Geometric constraints on the volume of remnant, midlatitude debris-covered glaciers. *Journal of Geophysical Research: Planets*, *119*, 2188–2196. https://doi.org/10.1002/2014JE004685

Madeleine, J.-B., Forget, F., Head, J. W., Levrard, B., Montmessin, F., & Millour, E. (2009). Amazonian northern mid-latitude glaciation on Mars: A proposed climate scenario. *Icarus*, *203*, 390–405. https://doi.org/10.1016/j.icarus.2009.04.037

Madeleine, J. B., Forget, F., Millour, E., Navarro, T., & Spiga, A. (2012). The influence of radiatively active water ice clouds on the Martian climate. *Geophysical Research Letters*, *39*, L23202. https://doi.org/10.1029/2012GL053564

Malin, M. C., Bell, J. F. III, Cantor, B. A., Caplinger, M. A., Calvin, W. M., Clancy, R. T., et al. (2007). Context Camera investigation on board the Mars Reconnaissance Orbiter. *Journal of Geophysical Research*, *112*, E05S04. https://doi.org/10.1029/2006JE002808

Mangold, N. (2003). Geomorphic analysis of lobate debris aprons on Mars at Mars Orbiter Camera scale: Evidence for ice sublimation initiated by fractures. *Journal of Geophysical Research*, (E4), 108, 8021. https://doi.org/10.1029/2002JE001885

Mangold, N. (2011). Ice sublimation as a geomorphic process: A planetary perspective. *Geomorphology*, *126*, 1–17. https://doi.org/10.1016/j.geomorph.2010.11.009

Mangold, N. (2012). Fluvial landforms on fresh impact ejecta on Mars. *Planetary and Space Science*, *62*(1), 69–85. https://doi.org/10.1016/j.pss.2011.12.009

McEwen, A. S., Eliason, E. M., Bergstrom, J. W., Bridges, N. T., Hansen, C. J., Delamere, W. A., et al. (2007). Mars Reconnaissance Orbiter's High Resolution Imaging Science Experiment (HiRISE). *Journal of Geophysical Research*, *112*, E05S02. https://doi.org/10.1029/2005JE002605

Mellon, M. T., Arvidson, R. E., Sizemore, H. G., Searls, M. L., Blaney, D. L., Cull, S., et al. (2009). Ground ice at the Phoenix landing site: Stability state and origin. *Journal of Geophysical Research*, *114*, E00E07. https://doi.org/10.1029/2009JE003417

Michael, G. G. (2013). Planetary surface dating from crater size–frequency distribution measurements: Multiple resurfacing episodes and differential isochron fitting. *Icarus*, *226*(1), 885–890. https://doi.org/10.1016/j.icarus.2013.07.004

Michael, G. G., Kneissl, T., & Neesemann, A. (2016). Planetary surface dating from crater size-frequency distribution measurements: Poisson timing analysis. *Icarus*, *277*, 279–285. https://doi.org/10.1016/j.icarus.2016.05.019

Michael, G. G., & Neukum, G. (2010). Planetary surface dating from crater size-frequency distribution measurements: Partial resurfacing events and statistical age uncertainty. *Earth and Planetary Science Letters*, *294*, 223–229. https://doi.org/10.1016/j.epsl.2009.12.041

Milliken, R. E., Mustard, J. F., & Goldsby, D. L. (2003). Viscous flow features on the surface of Mars: Observations from high-resolution Mars Orbiter Camera (MOC) images. *Journal of Geophysical Research*, (E6), 108, 5057. https://doi.org/10.1029/2002JE002005

Mischna, M. A., Richardson, M. I., Wilson, R. J., & McCleese, D. J. (2003). On the orbital forcing of Martian water and CO_2 cycles: A general circulation model study with simplified volatile schemes. *Journal of Geophysical Research*, *108*(E6), 5062. https://doi.org/10.1029/2003JE002051

Mungas, G. S., Rapp, D., Easter, R. W., Kenneth, R. J., & Wilson, T. (2006). Sublimation extraction of Mars H2O for future in-situ resource utilization. In *Earth & Space 2006: Engineering, Construction, and Operations in Challenging Environment* (pp. 1–8). League City/Houston, Texas: United States Publisher. https://doi.org/10.1061/40830(188)75

Murchie, S., Arvidson, R., Bedini, P., Beisser, K., Bibring, J. P., Bishop, J., et al. (2007). Compact Reconnaissance Imaging Spectrometer for Mars (CRISM) on Mars Reconnaissance Orbiter (MRO). *Journal of Geophysical Research*, *112*, E05S03. https://doi.org/10.1029/2006JE002682

Mustard, J. F., Cooper, C. D., & Rifkin, M. K. (2001). Evidence for recent climate change on Mars from the identification of youthful near-surface ground ice. *Nature*, *412*, 411–414.

Parsons, R., & Holt, J. (2016). Constraints on the formation and properties of a Martian lobate debris apron: Insights from high-resolution topography, SHARAD radar data, and a numerical ice flow model. *Journal of Geophysical Research: Planets*, *121*, 432–453. https://doi.org/10.1002/2015JE004927

Pierazzo, E., Artemieva, N. A., & Ivanov, B. A. (2005). Starting conditions for hydrothermal systems underneath Martian craters: Hydrocode modeling. In T. Kenkmann, F. Hörz, & A. Deutsch (Eds.), *Large meteorite impacts III*, *Geological Society of America Special Paper* (Vol. 384, pp. 443–457). https://doi.org/10.1130/0-8137-2384-1.443

Plaut, J. J., Safaeinili, A., Holt, J. W., Phillips, R. J., Head, J. W., Seu, R., et al. (2009). Radar evidence for ice in lobate debris aprons in the mid-northern latitudes of Mars. *Geophysical Research Letters*, *36*, L02203. https://doi.org/10.1029/2008GL036379

Rettberg, P., Anesio, A. M., Baker, V. R., Baross, J. A., Cady, S. L., Detsis, E., et al. (2016). Planetary protection and Mars special regions—A suggestion for updating the definition. *Astrobiology*, *16*(2), 119–125. https://doi.org/10.1089/ast.2016.1472

Senft, L. E., & Stewart, S. T. (2008). Impact crater formation in icy layered terrains on Mars. *Meteoritics & Planetary Science*, *43*(12), 1993–2013. https://doi.org/10.1111/j.1945-5100.2008.tb00657.x

Seu, R., Phillips, R. J., Biccari, D., Orosei, R., Masdea, A., Picardi, G., et al. (2007). SHARAD sounding radar on the Mars Reconnaissance Orbiter. *Journal of Geophysical Research*, *112*, E05S05. https://doi.org/10.1029/2006JE002745

Sherburn, J. A., & Horstemeyer, M. F. (2010). Hydrodynamic modeling of impact craters in ice. *International Journal of Impact Engineering*, *37*(1), 27–36. https://doi.org/10.1016/j.ijimpeng.2009.07.001

Smith, I. B., Putzig, N. E., Holt, J. W., & Phillips, R. J. (2016). An ice age recorded in the polar deposits of Mars. *Science*, *352*(6289), 1075–1078. https://doi.org/10.1126/science.aad6968

Souness, C., Hubbard, B., Milliken, R. E., & Quincey, D. (2012). An inventory and population-scale analysis of martian glacier-like forms. *Icarus*, *217*, 243–255. https://doi.org/10.1016/j.icarus.2011.10.020

Squyres, S. W. (1978). Martian fretted terrain: Flow of erosional debris. *Icarus*, *34*(3), 600–613. https://doi.org/10.1016/0019-1035(78)90048-9

Squyres, S. W. (1979). The distribution of lobate debris aprons and similar flows on Mars. *Journal of Geophysical Research*, *84*(B14), 8087–8096. https://doi.org/10.1029/JB084iB14p08087

Squyres, S. W., & Carr, M. H. (1986). Geomorphic evidence for the distribution of ground ice on Mars. *Science*, *231*, 249–252. https://doi.org/10.1126/science.231.4735.249

Stuurman, C. M., Osinski, G. R., Holt, J. W., Levy, J. S., Brothers, T. C., Kerrigan, M., & Campbell, B. A. (2016). SHARAD detection and characterization of subsurface water ice deposits in Utopia Planitia, Mars. *Geophysical Research Letters*, *43*, 9484–9491. https://doi.org/10.1002/2016GL070138

Viola, D., & McEwen, A. S. (2018). Geomorphological evidence for shallow ice in the southern hemisphere of Mars. *Journal of Geophysical Research: Planets*, *123*, 262–277. https://doi.org/10.1002/2017JE005366

Wasilewski, T. G. (2018). Evaluation of drilling-based water extraction methods for Martian ISRU from mid-latitude ice resources. *Planetary and Space Science*, *158*, 16–24. https://doi.org/10.1016/j.pss.2018.05.012

Weiss, D. K., & Head, J. W. (2016). Impact ejecta-induced melting of surface ice deposits on Mars. *Icarus*, *280*(Supplement C), 205–233. https://doi.org/10.1016/j.icarus.2016.07.007

Williams, N. R., Bell Iii, J. F., Christensen, P. R., & Farmer, J. D. (2015). Evidence for an explosive origin of central pit craters on Mars. *Icarus*, *252*, 175–185. https://doi.org/10.1016/j.icarus.2014.12.005

Zuber, M. T., Smith, D. E., Solomon, S. C., Muhleman, D. O., Head, J. W., Garvin, J. B., et al. (1992). The Mars Observer laser altimeter investigation. *Journal of Geophysical Research*, *97*(E5), 7781–7797. https://doi.org/10.1029/92JE00341